Observation of dynamic screening in the excited exciton states in multilayered MoS_2

Manobina Karmakar,[1] Sayantan Bhattacharya,[1,*] Subhrajit Mukherjee,[2,†] Barun Ghosh,[3] Rup Kumar Chowdhury,[1] Amit Agarwal,[3] Samit Kumar Ray,[1,4] Debashis Chanda,[5,6,7,‡] and Prasanta Kumar Datta[1,§]

[1]*Department of Physics, Indian Institute of Technology Kharagpur, Kharagpur 721302, India*
[2]*Advanced Technology and Development Centre, Indian Institute of Technology Kharagpur, Kharagpur 721302, India*
[3]*Department of Physics, Indian Institute of Technology - Kanpur, Kanpur 208016, India*
[4]*S. N. Bose National Centre for Basic Sciences, Kolkata 700106, India*
[5]*NanoScience Technology Center, Department of Physics and CREOL, The College of Optics and Photonics, University of Central Florida, Orlando, Florida 32826, USA*
[6]*CREOL, The College of Optics and Photonics, University of Central Florida, Orlando, Florida 32816, USA*
[7]*Department of Physics, University of Central Florida, Orlando, Florida 32816, USA*

(Received 18 May 2020; revised 6 February 2021; accepted 11 February 2021; published 23 February 2021)

Excitonic resonance and binding energies can be altered by controlling the environmental screening of the attractive Coulomb potential. Although this screening response is often assumed to be static, the time evolution of the excitonic quasiparticles manifests a frequency dependence in its Coulomb screening efficacy. In this paper, we investigate a ground (1s) and first excited exciton state (2s) in a multilayered transition metal dichalcogenide (MoS_2) upon ultrafast photoexcitation. We explore the dynamic screening effects on the latter and show its resonance frequency is the relevant frequency at which screening from the smaller-sized 1s counterparts is effective. Our finding sheds light on new avenues of external tuning on excitonic properties.

DOI: 10.1103/PhysRevB.103.075437

I. INTRODUCTION

Excitons or Coulomb-bound electron-hole pairs in semiconductors possess a potential for faster optical communication due to the efficient light-matter coupling and higher packing density compared to conventional electronics [1,2]. The fundamental interaction that alters the bound state of an electron-hole pair is screening or attenuation of the Coulomb potential in presence of neighboring charge carriers which includes but not limited to atoms (dielectric screening), free carriers, excitons, and plasma. Enhanced screening leads to reduced exciton oscillator strength and binding energy [3,4]. A plethora of experimental studies utilize this ubiquitous phenomenon to realize external control of the excitonic states through photoexcitation [5], carrier injection [4], and modification of the dielectric environment [6–9]. However, the theoretical formulations that account for screening quantitatively are long-sought and well-debated [10–13]. While many of the previous studies consider long-wavelength (static) response of the environmental macroscopic polarization to account for the experimental results, static approximation largely overestimates the screening efficiency of the quasiparticles leading to inconsistencies between experimental and theoretical binding energies, oscillator strengths, Mott density, etc. [13,14] The sole reason is that static polarization responses from the surrounding charge-carrying particles are too slow to screen the excitonic Coulomb field that evolve at much faster timescales [13].

The excitons are continuously annihilated and recreated through exchange interactions [15] and scattered to free carriers [16–18]; therefore, the Coulomb potential that binds the excitons is not static in time. Some recent theoretical studies indicate certain "characteristic frequencies" at which exciton screening is predominant [13,19]. Nevertheless, one major bottleneck in the understanding of the dynamic nature of Coulomb screening is the severe lack of experimental evidence. Therefore the characteristic frequency (or frequencies) is an open question to date. Apart from clarity in the underlying physics, an effective device engineering necessitates comprehension of the dynamic screening effects in excitons.

Motivated by this, we explore the free-carrier and exciton-induced screening effects in excitons using ultrafast transient absorption spectroscopy that allows us to probe the temporal evolution of the screening. We choose multilayered Molybdenum di-sulfide (MoS_2), a widely studied transition metal dichalcogenide (TMDC) material that offers stable, room-temperature excitons, which are also prone to sizable Coulomb screening owing to the layered architecture [20]. We track the photoinduced evolution of the ground (1s) and first excited (2s) excitonic states. Importantly, we observe an enhancement in the 2s exciton absorption oscillator strength followed by photoexcitation. This observation is in sharp contrast to plethora of time-resolved studies that report photo-induced reduction of excitonic oscillator strength due to state

*Present address: Department of Chemistry, University of Sheffield, Sheffield S3 7HF, United Kingdom.
†Present address: Faculty of Materials Science & Engineering, Technion - Israel Institute of Technology, Haifa, Israel - 3203003.
‡Debashis.Chanda@ucf.edu
§pkdatta@phy.iitkgp.ac.in

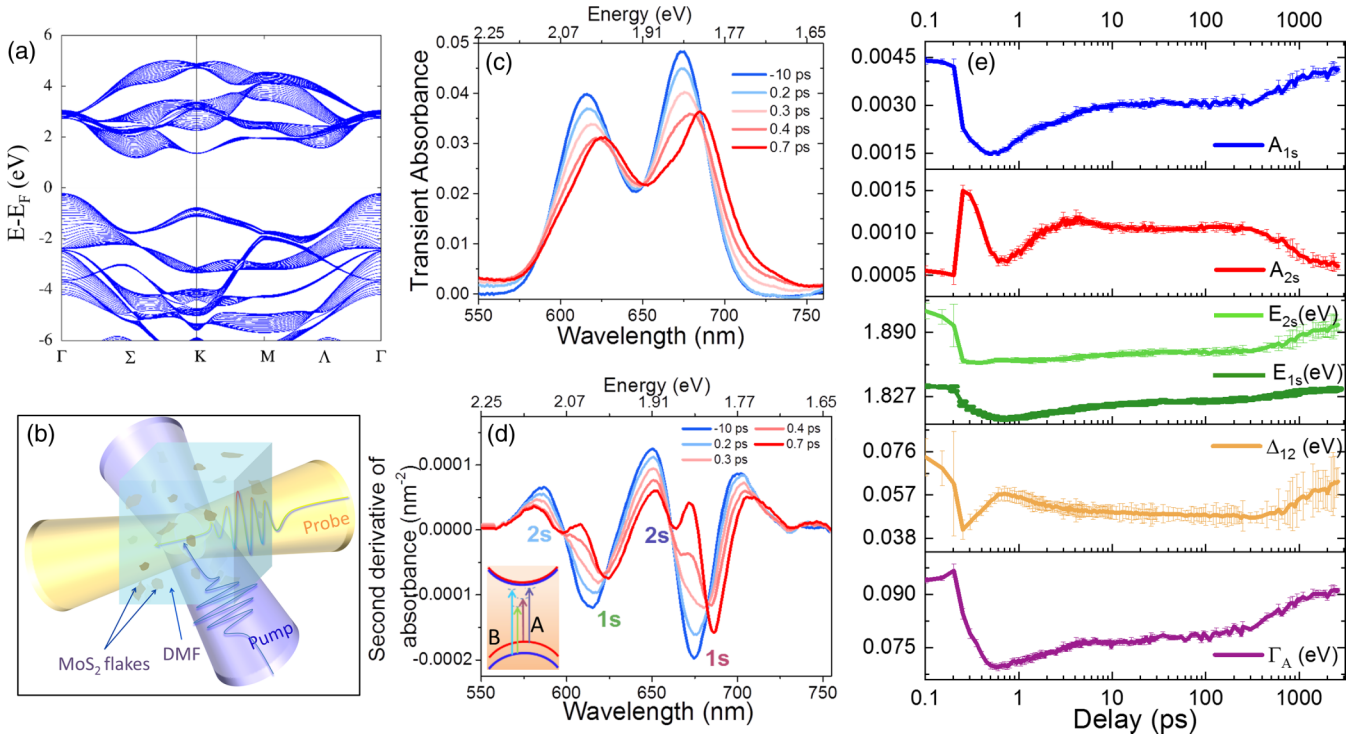

FIG. 1. (a) Quasiparticle bandstructure of 20-layered MoS_2. (b) Schematic of the multilayered, dispersed TMDC and ultrafast light-matter interaction. (c) Absorbance [$A_{pump}(\lambda)$] of multilayered MoS_2 flakes at different probe delays for a pump fluence of 11 $\mu J/cm^2$, showing the A and the B exciton resonance (d) The second-derivative of $A_{pump}(\lambda)$ (with respect to λ) at different probe delays. The inset shows a schematic of the 1s and 2s excitonic states of both A and B resonances. (e) Temporal-evolution of various excitonic parameters related to ground and first excited state of A exciton, namely exciton oscillator strength, resonance energy, 1s-2s resonance energy separation, and exciton linewidth upon 415 nm pump-excitation.

filling and/or, screening followed in different semiconductors. We model the excitation-induced changes in the intrinsic dielectric permittivity (DEP) and reveal a reduction in the frequency-dependent (dynamic) effective dielectric permittivity of the 2s state, which triggers the enhanced absorption in the particular state. Precisely, the 2s excitons are sensitive to the intrinsic DEP dictated by 1s excitons at the 2s resonant frequency. This observation provides first-ever experimental evidence towards the perception of exciton-induced dynamic screening in semiconductors.

II. RESULTS AND DISCUSSIONS

Linear absorption spectrum of sono-chemically exfoliated multilayered MoS_2 [21] (Ref. [22], Secs. S1 and S2) depicts the well-known A and B excitonic features centered around 674 nm (1.84 eV) and 614 nm (2.02 eV). Quasiparticle band-structure calculations (see Ref. [22], Sec. S3) of the multilayered TMDC using *GW* method is presented in Fig. 1(a).

We study ultrafast transient absorption spectra of MoS_2 flakes obtained using a 415 nm (2.98 eV) pump excitation and a CaF_2 generated broadband supercontinuum probe pulse and a variable pump-probe delay up to 3 ns. A schematic illustration of the light-matter interaction is depicted in Fig. 1(b). Figure 1(c) reveals the background-corrected transient probe absorbance (see Ref. [22], Sec. S5 for details) or $A_{pump}(\lambda)$, at a few selected probe delays (0.2–0.7 ps) and that without pump-excitation (−10 ps). With increasing probe delay, we observe red-shifted A and B absorption along with an aberrant distortion in the spectral shape of each exciton at the higher energy side. To resolve any small spectral features, we plot the second-derivative of the absorption data in Fig. 1(d). The derivative spectrum at −10 ps delay looks symmetric, whereas, at higher delays, the spectrum deviates significantly at the lower wavelength side of each exciton. This observation indicates appearance or enhancement of additional features other than the A and B ground states followed by photoexcitation. The possibility of observing higher-order quasiparticles (trions or biexcitons) are precluded, as they lie on the higher wavelength side of the excitonic features [23]. A possible artifact of photoinduced lattice heating is the appearance of phonon sidebands [24]. We perform temperature-dependent linear absorption to identify phonon sidebands at an elevated temperature (Fig. S2.2, Ref. [22]). However, no asymmetry or kink appears at the higher-energy side of each exciton. The possibility of interlayer excitons [25] is also ruled out (see Ref. [22], Sec. S11). Consequently, we assign these new features to the first excited states of excitons (2s excitonic states) (also see Ref. [22], Sec. S12). We fit the derivative spectrum of the absorption data in the absence of pump and identify the 2s states of A excitons centered around 648 nm (1.91 eV) having a spectral weight $\sim 1/8$ that of 1s state, as predicted [26]. From the spectral positions, we estimate exciton binding energy of 0.1 ± 0.007 eV of A,1s excitons [27,28]. Earlier reports on bulk and multilayered TMDC [29–31] estimate similar values.

Temporal behavior of the various parameters including exciton oscillator strength (OS), energy resonance, linewidth, 1s-2s energy separation are found by fitting the second-order derivative (with respect to wavelength λ) of transient probe absorbance with the second-order derivative of the Gaussian-convoluted Elliott formula [26] in Eq. (1).

$$\frac{d^2A_{\text{pump}}(\lambda)}{d\lambda^2} = \frac{d^2}{d\lambda^2}\left[\sum_{i=A,B}\sum_{j=1s,2s}\frac{A_{ij}}{\Gamma_{ij}}e^{-\frac{\hbar^2c^2}{\Gamma_{ij}^2}(\frac{1}{\lambda}-\frac{1}{\lambda_{ij}})^2}\right]. \quad (1)$$

Here, A_{ij} is the normalized amplitude of the Gaussian (oscillator strength), Γ_{ij} is the linewidth and λ_{ij} is the exciton peak wavelength. Figure S6 in Ref. [22] explicitly shows the excellent fitting of Eq. (1) with the data by retaining only the 1s and 2s excitons for the A and only 1s excitons for B resonances. Extracted parameters for both ground and first excited states of A exciton for varying probe-delays are presented in Fig. 1(e). The oscillator strength A_{1s} corresponding to 1s state shows reduction suggesting Pauli-blocking and screening due to pump-induced quasiparticles [32]. We observe two exponential decay components τ_1 ($\sim$1 ps) and τ_2 ($\sim$1 ns) dictate the dynamics and are assigned to nonradiative carrier scattering [33] and radiative exciton recombination [34,35], respectively (see Ref. [22], Sec. S7). In contrast to the 1s state, we find an enhanced absorption oscillator-strength for the 2s state, which eventually reverses to the steady-state value after a few ns. Such absorption enhancement indicates an effective increase in binding energy. This is in contrast to well-known Pauli blocking or screening-induced binding energy reduction of excitons followed by photoexcitation. We will discuss this in detail.

Moreover, pump-induced charge carriers renormalize the repulsive potential energy (self-energy) and reduce the single-particle band gap, leading to a lowering of the exciton resonance energies (δ_r) [4,32,36]. Simultaneously, the screening of the attractive interaction between the exciton constituents, reduces binding energy, making it blue-shifted towards the conduction band edge: $E_j \rightarrow E_j - \delta_r + \delta_b|_j$, where $E_j = \frac{hc}{\lambda_j}$, $j =$ 1s and 2s [36]. For a locally screened Coulomb potential, $\delta_b|_{1s} > \delta_b|_{2s}$ (see Ref. [22], Sec. S10). Consequently, a higher redshift in the 2s state is observed.

Moreover, the excitonic linewidth is narrowed by 24 meV, followed by the pump-excitation. A plausible reason is the increase in the exciton coherence lifetime owing to Pauli-blocking of the momentum-dark states [37,38] (see Ref. [22], Sec. S8 for a detailed discussion).

Having an overall idea on the time evolution of the excitonic properties, we turn to investigate the screening and 2s exciton oscillator-strength enhancement. Locally screened, three-dimensional hydrogen model [27] describes the tuning of Coulomb interaction of an electron-hole pair by employing an effective permittivity experienced by the excitons for n^{th} state:

$$\epsilon_r|_n{}^2 = \frac{\mu e^4}{(4\pi\epsilon_0)^2 2\hbar^2 n^2 E_b|_n}, \quad (2)$$

where $E_b|_n$ is exciton binding energy of nth exciton state, μ is exciton effective mass and $\epsilon_r|_n$ is effective dielectric constant. This quantity ϵ_r summarizes all Coulomb screening effects experienced by an electron-hole pair [28]. If we consider an oversimplified picture of an exciton, where an electron and hole pair is a static entity in real space and time, the static DEP of the environment will describe the screening interactions sufficiently. However, several timescales are associated with the excitons owing to many-body interactions in semiconductors. Excitons are neither static in space nor in time. Though electronic transitions are considered instantaneous (at least with respect to the present technology), the Coulomb correlation formation is not instantaneous. Huber *et al.* in their phenomenal study in 2001, have directly observed coherent plasmon formation, where the Coulomb-correlated many-particle state builds up in a time related to the inverse of the plasma frequency [39]. With that, it would only be a conjecture to assume the Coulomb correlation between an electron and hole pair forms in a time related to the inverse of excitonic resonance. Also, excitons get ionized to free carriers, scattered to momentum-dark states through phonon interactions. Electron-hole exchange interaction takes place, leading to spin relaxation of excitons [15,40]. Each of these processes have their specific timescales. Accordingly, the medium surrounding an exciton screens the electron-hole interactions at those particular frequencies. Polarizability response of the environment at other frequencies are either too slow or too fast to affect the Coulomb interactions significantly. Importantly, Steinhoff *et al.* discuss an effective exciton screening specifically at its binding energy since bound exciton to free electron-hole plasma scattering occurs at this energy [19]. Therefore the frequency dependence of the environmental permittivity needs to be considered to describe the Coulomb screening of excitons.

In the case of an ideal two-dimensional semiconductor, the environmental screening of an exciton includes the substrate response and a minimal response from the semiconducting layer itself. For a three-dimensional system like the one we study, the field lines joining an electron and a hole are essentially within the same material [see Fig. 2(b), right panel]. Hence, the screening of the Coulomb field is predominantly from the surrounding layers.

In our experimental conditions, pump-induced exciton and carrier population modify the charge environment of the 2s excitons such that its oscillator strength is enhanced. This observation is indicative of reduced screening and therefore, reduced effective permittivity. Static screening by free carriers fails to explain it, and we need to consider the dynamic screening in the TMDC. Yet, it is almost an improbable task to determine an exciton's effective permittivity ($\epsilon_r|_n$) from the full frequency-dependent material dielectric permittivity of the environment. A reliable model on the same is not available. Here, we propose a phenomenological model based on the effectiveness of the screening at different frequencies of the electromagnetic spectrum. The effective permittivity of an exciton state in Eq. (2) is expressed in terms of the environmental dielectric permittivity $\epsilon_r(\omega)$ as

$$\epsilon_r|_n = \frac{\int_0^\infty W(\omega)\epsilon_r(\omega)d\omega}{\int_0^\infty W(\omega)d\omega}. \quad (3)$$

As we discussed earlier, some particular frequencies are more effective than the other. In Fig. 2(b), left panel, we sketch the

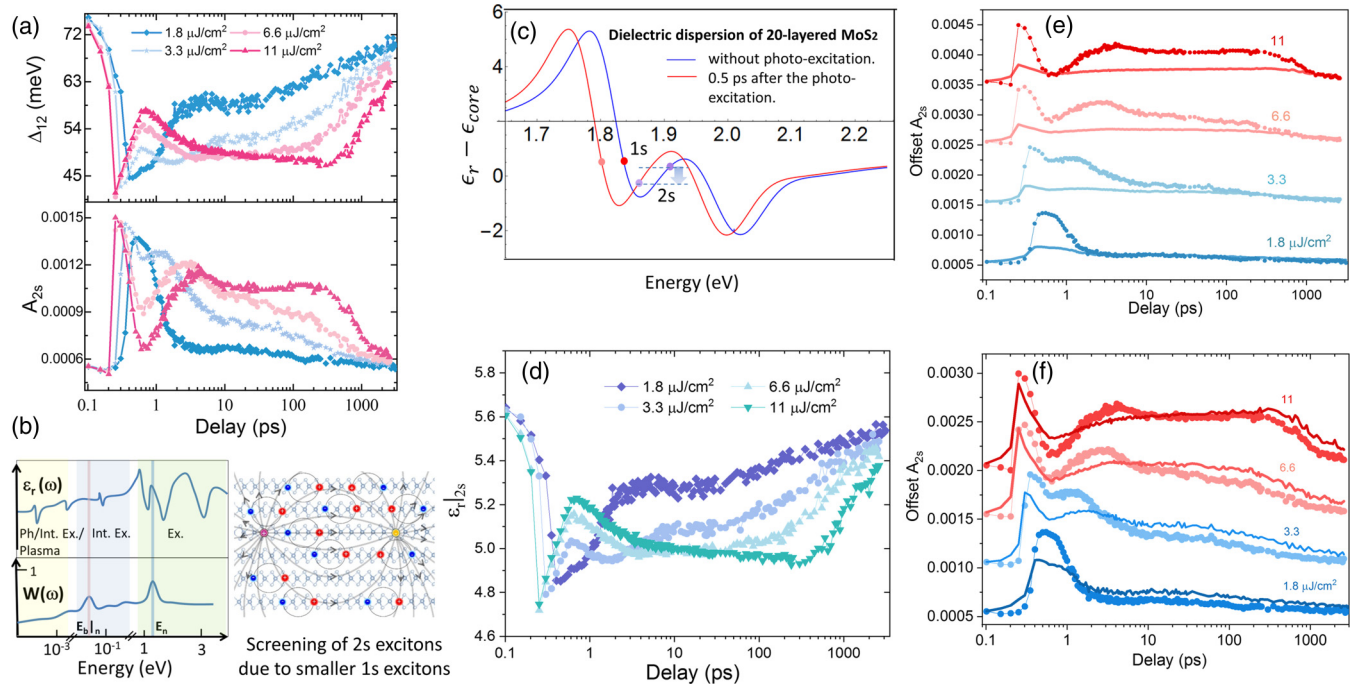

FIG. 2. (a) Temporal evolution of 1s-2s resonance energy separation (Δ_{12}) and the absorption oscillator strength of 2s excitons (A_{2s}). (b) (Left) A pedagogical, schematic illustration of the effectiveness of the screening [$W(\omega)$] and DEP [$\epsilon_r(\omega)$] of MoS_2 over a broad energy range. The dielectric function below 10^{-3} eV is dominated by phonons (Ph), interexcitonic transitions (Int. Ex.), and plasma, whereas excitons (Ex.) dominate the spectrum at few eV range. (Right) A schematic of the 1s (red-blue circle) and 2s excitons (purple-yellow circles). Field lines joining the latter penetrates the 1s excitons which contribute to screening. (c) Exciton-induced permittivity of 20-layered MoS_2 estimated using the Kramers-Kronig relations. Blue and red curves display the dispersion for an unexcited condition, and 0.5 ps after pump excitation (with a fluence of 5.5 μ J/cm^2). 1s and 2s excitonic positions are indicated by red and purple filled circles. An arrow indicates the drop of permittivity at 2s resonance in the photoexcited case. (d) Temporal variation of the effective permittivity of 2s resonance at four different pump fluences. (e) Temporal variation of 2s state oscillator strength for different pump fluences. Experimentally obtained values (same as (a), lower panel) are presented as scatter plots, and the solid lines are the estimated values from Eqs. (2) and (4). (f) Similar to (e), with minimized mean-squared error with respect to scaling of A and B, 1s absorption oscillator strength.

frequency-dependent effectiveness [$W(\omega)$] and the environmental (intrinsic) DEP for pedagogical purposes.

It is evident that static dielectric permittivity increases due to the pump-induced elevated population of charge carriers. Also, the plasma frequencies owing to the carrier injection is estimated at $\sim 10^{-2}$ meV, much less than the 2s exciton binding energy ($\sim$25 meV). Therefore, the effective permittivity of 2s states reduces neither at static limits nor at the binding energy range. Next, we explore the material DEP evolution at the visible optical frequencies, especially at 2s exciton resonance.

We note that both 1s and 2s excitons undergo red-shift with probe delay. We present the delay-dependent 1s-2s resonance energy separation (Δ_{12}) in Fig. 2(a), upper panel for four different pump fluences. Notably, Δ_{12} reduces by $\sim$30 meV for pump fluence of 11 μ J/cm^2. The nontrivial temporal variation remains nonintuitive at this point. We also plot A_{2s} in the lower panel. Unlike other quantities, the reversion dynamics of both A_{2s} and Δ_{12} are nonmonotonic with delay and show much variation. Notably, the nonmonotonic dynamics of A_{2s} and Δ_{12} seem to be inversely correlated, with the maxima in A_{2s} temporally coinciding with the minima in Δ_{12}.

To understand the frequency-dependent material DEP, we employ the Kramers-Kronig (KK) relation [41] based on the linear absorbance data in the visible region (see Ref. [22], section S9) to find out the real part of the dielectric dispersion ($\epsilon_{r,\mathrm{KK}}(\lambda) = \epsilon_r - \epsilon_{\mathrm{core}}$) due to excitonic transitions. Note that, material DEP is given by $\epsilon_{r,\mathrm{KK}}(\lambda) + \epsilon_{\mathrm{core}}$, where ϵ_{core} is a nearly frequency-invariant background permittivity originating from interband transitions. As we use TMDC flakes in dispersion, with probe beam size ($\sim$80 μm beam diameter) being few-orders larger than the individual suspended flakes, the experimentally measured absorbance is less than the actual absorbance of a 20-layered MoS_2 flake. Therefore we estimate a scaling parameter (5 ± 2) of the absorbance by extrapolating an earlier work [9] (see Ref. [22], Sec. S9). Hereby, we plot the exciton-induced DEP with (for a probe delay of 0.5 ps) and without photoexcitation in Fig. 2(c) using the corresponding experimentally obtained E_{2s} and E_{1s} values in the KK equation. We identify the 1s and 2s resonance energies by red and purple filled circles in the figure. We observe a reduced material permittivity at the redshifted 2s resonance energy. This observation encourages us to trace the probe-delay dependent variation of effective permittivity at the varying 2s resonance and its relation with A_{2s} enhancement.

Following Eq. (2), we extract the effective exciton permittivity of 5.7 (in absence of pump excitation) with calculated exciton reduced mass of $0.24m_0$. Next, we utilize our model to estimate delay-dependent effective exciton permittivity upon photoexcitation. In the present study, plasma frequency is

nonresonant with exciton binding energy to show any nontrivial variation [19], and photoexcitation leads to increased material DEP at the static limit. Hence, the observed effective permittivity reduction of the 2s states cannot be related to the material DEP at these frequency regimes. Accordingly, we assume that effective permittivity reduction is dominantly dictated by the material DEP reduction at exciton resonance (i.e, $W(\omega_{2s}) \gg W(\omega \neq \omega_{2s})$. Hence, we separate the effective permittivity of the 2s excitons into two components-(i) permittivity at exciton resonance due to 1s excitons (ii) a core permittivity ($\epsilon_{\text{core}}|_{2s}$) due to other interband transitions as a cumulative effect from all frequencies other than the resonance. While the first term evolves with photoexcitation, the other is assumed to be fixed. This assumption is valid because we restrict our experiments to low excitation densities ensuring interband transitions are not modified significantly (see Fig. S5.3, Ref. [22]). We calculate the contribution of nonvarying core effective permittivity, that is $\epsilon_{\text{core}}|_{2s}$, by the difference of effective exciton permittivity and material DEP at the 2s resonance in absence of photoexcitation. Next, we trace the delay-dependent effective permittivity of the 2s resonance ($\varepsilon_r|_{2s}$) and plot in Fig. 2(d). Temporal evolution of this quantity shows similar dynamics inversely related to the nontrivial, nonmonotonic variation of A_{2s}.

We note that the exciton oscillator strength (A_j) in a three dimensional semiconductor varies as $A_j \propto r_j^{-3}$, where r_j denotes the exciton radius [41]. The exciton radius, in turn, varies linearly with the effective permittivity [42], leading to

$$A_j \propto \epsilon_r^{-3}. \tag{4}$$

Thereafter, we calculate the temporal evolution of A_{2s} from $\epsilon_r|_{2s}$ [Fig. 2(d)] and depict the same for four different pump fluences in Fig. 2(e). Remarkably, the temporal evolution of the A_{2s} is well-reproduced qualitatively. However, calculated values underestimate experimental A_{2s}, almost by a factor of 1/2. This is improved by optimizing the scaling parameter by 40%, which lies within the standard error of the mentioned data extrapolation. Recalculated A_{2s} values displayed in Fig. 2(f) depicts a better quantitative estimation of the experimental data.

Our observation excellently demonstrates that reduced material DEP at the exciton resonance governs the oscillator strength enhancement of the 2s excitons. Coulomb attractive field of the electron-hole pair of the 2s exciton gets screened by its environment, which is the MoS_2 material itself [Fig. 2(b), right panel]. The 1s resonance dictate the material polarizability at the visible frequencies. Thus the primary source of screening response at the resonance frequency is the 1s excitons. Photoexcitation triggers reduced effective permittivity due to reduced 1s-2s energy separation, which facilitates reduced screening or "antiscreening" [43] leading to the enhanced exciton oscillator strength. As we demonstrated in Fig. 2(c), the reduction of Δ_{12} plays a pivotal role here. As this anti-screening is dictated by the Δ_{12}, this effect has an upper-limit pertaining to the 2s exciton resonance entering anomalous dispersion region of 1s exciton oscillator. For example, consider the DEP at 0.5 ps delay in Fig. 2(c). The photoinduced 2s exciton position is around 1.85 eV; however, if it reaches 1.82 eV (for more intense photoexcitation),

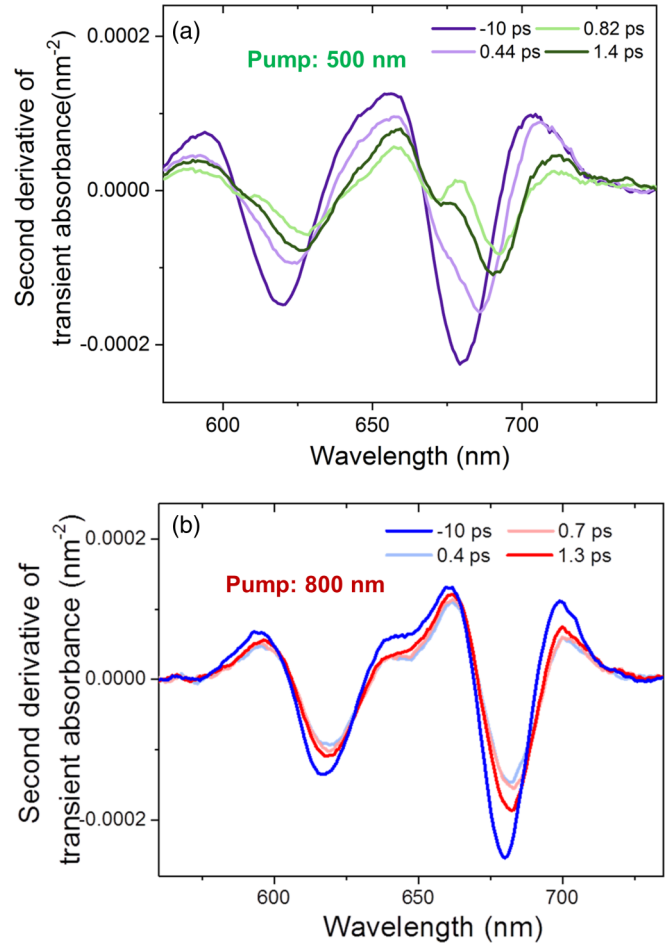

FIG. 3. Second-order derivative of the transient absorbance spectra at a few selected delays after photoexcitation with (a) 500-nm and (b) 800-nm pump of fluence of 6 and 264 μJ/cm^2, respectively. Additional kinks owing to enhanced 2s exciton absorption are indicated in case of 500-nm pump excitation. This remains absent for below-resonance excitation at 800 nm.

further red-shift of the state would increase the material DEP at the resonance (see Ref. [22], Sec. S10 for some additional discussion).

We repeat the pump-probe experiments with thin films of multilayered flakes on quartz substrates. We excite the sample linearly with 500-nm and 800-nm pump and observe the resulting second-derivative of the transient absorption at a few selected probe delays in Figs. 3(a) and 3(b). We observe additional kinks upon pump excitation at the lower-wavelength sides of the A and B, 1s excitons followed by 500-nm excitation, similar to Fig. 1(e) for 415-nm excitation. Interestingly, such additional kinks in the absorption derivative is not observed for 800-nm photoexcitation. As depicted earlier, the kinks appear as a result of enhanced 2s exciton absorption. Note that, while 500-nm (2.48 eV) pump excitation is above the A and B, 1s resonance and thus, ensures generation of the same, only free carriers are formed followed by 800-nm (1.55 eV) excitation. Therefore the lack of 2s state enhancement in the absence of pump-induced 1s states reaffirms the role of photo-induced 1s excitons in the anti-screening and absorption enhancement of 2s excitons.

In this study, a quantitative understanding of dynamic exciton screening is established through a proposed model [Eq. (3)]. We have introduced a hypothesis of efficient screening at resonance [$W(\omega_{2s}) \gg W(\omega \neq \omega_{2s})$], guided by the experimental observation of reduced permittivity at the exciton resonance. This hypothesis, along with the proposed model quantitatively reproduces the aberrant oscillator strength dynamics of the 2s excitons. A full, generalized quantitative evaluation of the dynamic screening of excitons remains challenging and is beyond the scope of this work.

In conclusion, we report an interesting observation of photo-induced enhancement of exciton oscillator strength in contrary to the well-known exciton bleaching effects due to state-filling and free-carrier screening upon photoexcitation. This observation provides strong experimental evidence of dynamic Coulomb screening in excitons. We propose a phenomenological model for incorporating the environmental dielectric screening of excitons and reveal that environmental polarization response at the resonance effectively screens the excitons. In our experimental scenario, material dimension being much larger than exciton radius, the semiconductor material itself acts as the environment. Photoinduced 1s excitons significantly screen the 2s excitons. Photoexcitation leads to the renormalization of the exciton resonances. The material permittivity response of 1s excitons gets reduced at 2s resonance, and an "antiscreening" (reduced screening) in the 2s state is observed. This observation opens up new opportunities to tailor exciton resonances without losing the population, unlike existing approaches. An exhaustive quantitative analysis on the dynamic screening is a complicated problem and remains an open question. We envision further rigorous experimental and theoretical studies on this topic.

ACKNOWLEDGMENTS

M.K. thanks Simone Peli for helpful discussions. The authors gratefully acknowledge the SDGRI-UPM project of IIT Kharagpur for all the necessary equipment. The authors thank Abhinav Kala and Venu Gopal Achanta from Tata Institute of Fundamental Research, India, for providing a low-temperature absorption measurement of the multilayered MoS_2 sample.

[1] A. A. High, E. E. Novitskaya, L. V. Butov, M. Hanson, and A. C. Gossard, Control of exciton fluxes in an excitonic integrated circuit, Science **321**, 229 (2008).

[2] G. Grosso, J. Graves, A. T. Hammack, A. A. High, L. V. Butov, M. Hanson, and A. C. Gossard, Excitonic switches operating at around 100 K, Nat. Photonics **3**, 577 (2009).

[3] E. X. Ping and H. X. Jiang, Effect of charge-carrier screening on the exciton binding energy in $GaAs/Al_xGa_{1-x}As$ quantum wells, Phys. Rev. B **47**, 2101 (1993).

[4] A. Chernikov, A. M. van der Zande, H. M. Hill, A. F. Rigosi, A. Velauthapillai, J. Hone, and T. F. Heinz, Electrical Tuning of Exciton Binding Energies in Monolayer WS_2, Phys. Rev. Lett. **115**, 126802 (2015).

[5] A. Chernikov, C. Ruppert, H. M. Hill, A. F. Rigosi, and T. F. Heinz, Population inversion and giant bandgap renormalization in atomically thin WS_2 layers, Nat. Photonics **9**, 466 (2015).

[6] P. Steinleitner, P. Merkl, A. Graf, P. Nagler, K. Watanabe, T. Taniguchi, J. Zipfel, C. Schüller, T. Korn, A. Chernikov, S. Brem, M. Selig, G. Berghäuser, E. Malic, and R. Huber, Dielectric engineering of electronic correlations in a van der waals heterostructure, Nano Lett. **18**, 1402 (2018).

[7] M. M. Ugeda, A. J. Bradley, S.-F. Shi, F. H. da Jornada, Y. Zhang, D. Y. Qiu, W. Ruan, S.-K. Mo, Z. Hussain, Z.-X. Shen, F. Wang, S. G. Louie, and M. F. Crommie, Giant bandgap renormalization and excitonic effects in a monolayer transition metal dichalcogenide semiconductor, Nat. Mater. **13**, 1091 (2014).

[8] A. Raja, A. Chaves, J. Yu, G. Arefe, H. M. Hill, A. F. Rigosi, T. C. Berkelbach, P. Nagler, C. Schüller, T. Korn, C. Nuckolls, J. Hone, L. E. Brus, T. F. Heinz, D. R. Reichman, and A. Chernikov, Coulomb engineering of the bandgap and excitons in two-dimensional materials, Nat. Commun. **8**, 15251 (2017).

[9] A. Castellanos-Gomez, J. Quereda, H. P. van der Meulen, N. Agraït, and G. Rubio-Bollinger, Spatially resolved optical absorption spectroscopy of single- and few-layer MoS_2 by hyperspectral imaging, Nanotechnology **27**, 115705 (2016).

[10] L. J. Sham and T. M. Rice, Many-particle derivation of the effective-mass equation for the wannier exciton, Phys. Rev. **144**, 708 (1966).

[11] H. Haug and D. B. T. Thoai, Dynamical screening of excitons by free carriers, Phys. Status Solidi B **85**, 561 (1978).

[12] R. Zimmermann, Dynamical screening of the wannier exciton, Phys. Status Solidi B **48**, 603 (1971).

[13] M. M. Glazov and A. Chernikov, Breakdown of the static approximation for free carrier screening of excitons in monolayer semiconductors, Phys. Status Solidi B **255**, 1800216 (2018).

[14] E. J. Sie, A. Steinhoff, C. Gies, C. H. Lui, Q. Ma, M. Rösner, G. Schönhoff, F. Jahnke, T. O. Wehling, Y.-H. Lee, J. Kong, P. Jarillo-Herrero, and N. Gedik, Observation of exciton redshift-blueshift crossover in monolayer WS_2, Nano Lett. **17**, 4210 (2017).

[15] T. Yu and M. W. Wu, Valley depolarization due to intervalley and intravalley electron-hole exchange interactions in monolayer MoS_2, Phys. Rev. B **89**, 205303 (2014).

[16] S. Schmitt-Rink, D. S. Chemla, and D. A. B. Miller, Theory of transient excitonic optical nonlinearities in semiconductor quantum-well structures, Phys. Rev. B **32**, 6601 (1985).

[17] A. Steinhoff, M. Florian, M. Rösner, G. Schönhoff, T. O. Wehling, and F. Jahnke, Exciton fission in monolayer transition metal dichalcogenide semiconductors, Nat. Commun. **8**, 1166 (2017).

[18] S. W. Koch, W. Hoyer, M. Kira, and V. S. Filinov, Exciton ionization in semiconductors, Phys. Status Solidi B **238**, 404 (2003).

[19] A. Steinhoff, T. O. Wehling, and M. Rösner, Frequency-dependent substrate screening of excitons in atomically thin transition metal dichalcogenide semiconductors, Phys. Rev. B **98**, 045304 (2018).

[20] E. J. G. Santos and E. Kaxiras, Electrically driven tuning of the dielectric constant in MoS_2 layers, ACS Nano **7**, 10741 (2013).

[21] S. Mukherjee, R. Maiti, A. Midya, S. Das, and S. K. Ray, Tunable direct bandgap optical transitions in MoS_2 nanocrystals for photonic devices, ACS Photonics **2**, 760 (2015).

[22] See Supplemental Material at http://link.aps.org/supplemental/10.1103/PhysRevB.103.075437 for additional discussion on sample characterization, experimental techniques and data analysis.

[23] Y. Lin, X. Ling, L. Yu, S. Huang, A. L. Hsu, Y.-H. Lee, J. Kong, M. S. Dresselhaus, and T. Palacios, Dielectric screening of excitons and trions in single-layer MoS_2, Nano Lett. **14**, 5569 (2014).

[24] D. Christiansen, M. Selig, G. Berghäuser, R. Schmidt, I. Niehues, R. Schneider, A. Arora, S. M. de Vasconcellos, R. Bratschitsch, E. Malic, and A. Knorr, Phonon Sidebands in Monolayer Transition Metal Dichalcogenides, Phys. Rev. Lett. **119**, 187402 (2017).

[25] J. Horng, T. Stroucken, L. Zhang, E. Y. Paik, H. Deng, and S. W. Koch, Observation of interlayer excitons in $MoSe_2$ single crystals, Phys. Rev. B **97**, 241404(R) (2018).

[26] R. J. Elliott, Intensity of optical absorption by excitons, Phys. Rev. **108**, 1384 (1957).

[27] C. F. Klingshirn, *Semiconductor Optics* (Springer, Berlin, 2007).

[28] A. Chernikov, T. C. Berkelbach, H. M. Hill, A. Rigosi, Y. Li, O. B. Aslan, D. R. Reichman, M. S. Hybertsen, and T. F. Heinz, Exciton Binding Energy and Nonhydrogenic Rydberg Series in Monolayer WS_2, Phys. Rev. Lett. **113**, 076802 (2014).

[29] V. Jindal, S. Bhuyan, T. Deilmann, and S. Ghosh, Anomalous behavior of the excited state of the *a* exciton in bulk WS_2, Phys. Rev. B **97**, 045211 (2018).

[30] Y. Xie, S. Zhang, Y. Li, N. Dong, X. Zhang, L. Wang, W. Liu, I. M. Kislyakov, J.-M. Nunzi, H. Qi, L. Zhang, and J. Wang, Layer-modulated two-photon absorption in MoS_2: Probing the shift of the excitonic dark state and band-edge, Photon. Res. **7**, 762 (2019).

[31] B. L. Evans, P. A. Young, and R. W. Ditchburn, Optical absorption and dispersion in molybdenum disulphide, Proc. R. Soc. London A **284**, 402 (1965).

[32] E. A. A. Pogna, M. Marsili, D. De Fazio, S. Dal Conte, C. Manzoni, D. Sangalli, D. Yoon, A. Lombardo, A. C. Ferrari, A. Marini, G. Cerullo, and D. Prezzi, Photo-induced bandgap renormalization governs the ultrafast response of single-layer MoS_2, ACS Nano **10**, 1182 (2016).

[33] F. Ceballos, Q. Cui, M. Z. Bellus, and H. Zhao, Exciton formation in monolayer transition metal dichalcogenides, Nanoscale **8**, 11681 (2016).

[34] H. Shi, R. Yan, S. Bertolazzi, J. Brivio, B. Gao, A. Kis, D. Jena, H. G. Xing, and L. Huang, Exciton dynamics in suspended monolayer and few-layer MoS_2 2d crystals, ACS Nano **7**, 1072 (2013).

[35] M. Palummo, M. Bernardi, and J. C. Grossman, Exciton radiative lifetimes in two-dimensional transition metal dichalcogenides, Nano Lett. **15**, 2794 (2015).

[36] G. Wang, A. Chernikov, M. M. Glazov, T. F. Heinz, X. Marie, T. Amand, and B. Urbaszek, Colloquium: Excitons in atomically thin transition metal dichalcogenides, Rev. Mod. Phys. **90**, 021001 (2018).

[37] M. Selig, G. Berghäuser, A. Raja, P. Nagler, C. Schüller, T. F. Heinz, T. Korn, A. Chernikov, E. Malic, and A. Knorr, Excitonic linewidth and coherence lifetime in monolayer transition metal dichalcogenides, Nat. Commun. **7**, 13279 (2016).

[38] A. Raja, M. Selig, G. Berghäuser, J. Yu, H. M. Hill, A. F. Rigosi, L. E. Brus, A. Knorr, T. F. Heinz, E. Malic, and A. Chernikov, Enhancement of exciton-phonon scattering from monolayer to bilayer WS_2, Nano Lett. **18**, 6135 (2018).

[39] R. Huber, F. Tauser, A. Brodschelm, M. Bichler, G. Abstreiter, and A. Leitenstorfer, How many-particle interactions develop after ultrafast excitation of an electron-hole plasma, Nature **414**, 286 (2001).

[40] L. Guo, M. Wu, T. Cao, D. M. Monahan, Y.-H. Lee, S. G. Louie, and G. R. Fleming, Exchange-driven intravalley mixing of excitons in monolayer transition metal dichalcogenides, Nat. Phys. **15**, 228 (2019).

[41] H. Haug and S. W. Koch, *Quantum Theory of the Optical and Electronic Properties of Semiconductors*, 5th ed. (World Scientific, Singapore, 2009).

[42] S. V. Gaponenko, *Introduction to Nanophotonics* (Cambridge University Press, Cambridge, 2010).

[43] J. van den Brink and G. A. Sawatzky, Non-conventional screening of the coulomb interaction in low-dimensional and finite-size systems, Europhys. Lett. **50**, 447 (2000).